

# Structural phase transition and material properties of few-layer monochalcogenides

Mehrshad Mehboudi,<sup>1</sup> Benjamin M. Fregoso,<sup>2</sup> Yurong Yang,<sup>1</sup> Wenjuan Zhu,<sup>3</sup> Arend van der Zande,<sup>4</sup> Jaime Ferrer,<sup>5</sup> L. Bellaiche,<sup>1</sup> Pradeep Kumar,<sup>1</sup> and Salvador Barraza-Lopez<sup>1,\*</sup>

<sup>1</sup>*Department of Physics, University of Arkansas, Fayetteville, AR 72701, USA*

<sup>2</sup>*Department of Physics, University of California, Berkeley, CA, 94720, USA*

<sup>3</sup>*Department of Electrical and Computer Engineering,*

*University of Illinois at Urbana-Champaign, Urbana, IL 61801, USA*

<sup>4</sup>*Department of Mechanical Science and Engineering,*

*University of Illinois at Urbana-Champaign, Urbana, IL 61801, USA*

<sup>5</sup>*Departamento de Física, Universidad de Oviedo, Asturias, Spain*

(Dated: June 5, 2022)

Monochalcogenide monolayers undergo a phase transition from a rectangular onto a square unit cell at finite temperature  $T_c$ . Here, we study the nature of this transition in few-layer monochalcogenides and its consequences for material properties, focusing on GeSe and SnSe monolayers and bilayers as prototypical examples. Despite of the structural disorder, no in-gap states develop at  $T_c$ . Nevertheless, the spin polarization of the conduction valley along the  $\Gamma - Y$  direction becomes degraded with temperature. The  $Y$ - and  $X$ -points become effectively equivalent at  $T_c$ , and the optical absorption band edge becomes unpolarized as a result. The average magnitude of the electric dipole moment vanishes at the transition temperature as well. This comprehensive set of results uncovers temperature as a fundamental control knob for applications based on few-layer monochalcogenides.

PACS numbers: 73.21.Ac, 71.15.Pd, 71.15.Mb, 63.22.Dc, 65.40.De, 71.20.Nr

Few-layer monochalcogenides are a new platform for phenomena in low dimensional systems that is being intensely explored now [1–8]. Monolayers of these materials have a four-fold degenerate ground state [9] that leads to two-dimensional disorder at finite temperature ( $T$ ) [9–11]. Disorder at individual layers underpins the phase transition observed in bulk layered monochalcogenides [12–15].

The promise of these materials rests on potential applications at finite temperature, making it imperative to predict the evolution of their properties [1–7] under thermal variations. Does thermal disorder induce in-gap states? Is spin-splitting robust at room temperature? Can the valley degree of freedom be even defined at the transition temperature? How do mobility, optical absorption, and electric dipole properties evolve with temperature? These pressing questions for the development of this field are answered within the context of monolayers (MLs) and bilayers (BLs) of GeSe and SnSe here.

We begin by comparing the phase transition occurring in MLs with that in BLs. This is accomplished in Fig. 1 by displaying the temperature derivative of the average total energy  $\langle E \rangle$ , and the mean lattice constants  $\langle a_1 \rangle$ ,  $\langle a_2 \rangle$ .  $\langle E \rangle$  was obtained from NPT Carr-Parrinello molecular dynamics (MD) runs (on a fixed number of particles, at ambient pressure, and at finite temperature), as implemented in the *SIESTA* DFT code [16–18]. Calculations proceeded on  $8 \times 8$  supercells for about 1000 fs (and with a 1.0 fs time resolution) and employed standard basis sets [19], pseudopotentials with van der Waals corrections of the Berland-Per Hyldgaard type [20, 21], a k-point grid including the  $\Gamma$ -point, and a mesh cutoff of 150 Ry.  $\langle a_1 \rangle$

and  $\langle a_2 \rangle$  are averaged from over 128,000 (256,000) individual values from ML (BL) runs.

The peak in the specific heat when  $\langle a_1 \rangle = \langle a_2 \rangle$  defines the critical temperature  $T_c$ , and it is sharper in MLs than in BLs, implying the existence of an interplay between interlayer coupling and intra-layer disorder in the latter. The vertical solid lines on ML subplots indicate magnitudes of  $T_c$  close to 425 K for a GeSe ML and 200 K for the SnSe ML, that match predicted values [9] reasonably well [22]. According to Fig. 1, the temperature at which  $\langle a_1 \rangle = \langle a_2 \rangle$  is equal to 450 K for GeSe BLs and 375 K for SnSe BLs. Together with the larger value of  $T_c$  for bulk SnSe [12–14], the results in Fig. 1 indicate that  $T_c$  can be tuned by the number of layers.

The inset in the SnSe ML  $\Delta \langle E \rangle / \Delta T$  subplot shows the hallmark of the transition: a reassignment of nearest neighboring atoms –shown by thick dashed lines across the ridges– that induces in-plane strain, leading onto the 2D structure in which  $\langle a_1 \rangle$  and  $\langle a_2 \rangle$  are identical: The square unit cell –corresponding to a point of unstable equilibrium at 0 K [9]– becomes the preferred structure at  $T_c$ , on average.

The behavior of the fluctuations about the mean values of  $a_1$  and  $a_2$  in Fig. 1 led us to study the nature of the phase transition. The probability distribution  $\rho(a_1, a_2)$  on Fig. 2 obtained at various temperatures for GeSe and SnSe MLs (where  $\langle a_i \rangle = \int \rho(a'_1, a'_2) a'_i da'_1 da'_2$ , and  $i = 1, 2$ ) is inconsistent with a displacive transition where individual atomic displacements correlate up to mesoscopic distances. Indeed, at low temperatures  $a_1$  and  $a_2$  cluster towards their values at 0 K because bond recommitment is not thermally allowed. Excursions of  $a_1$

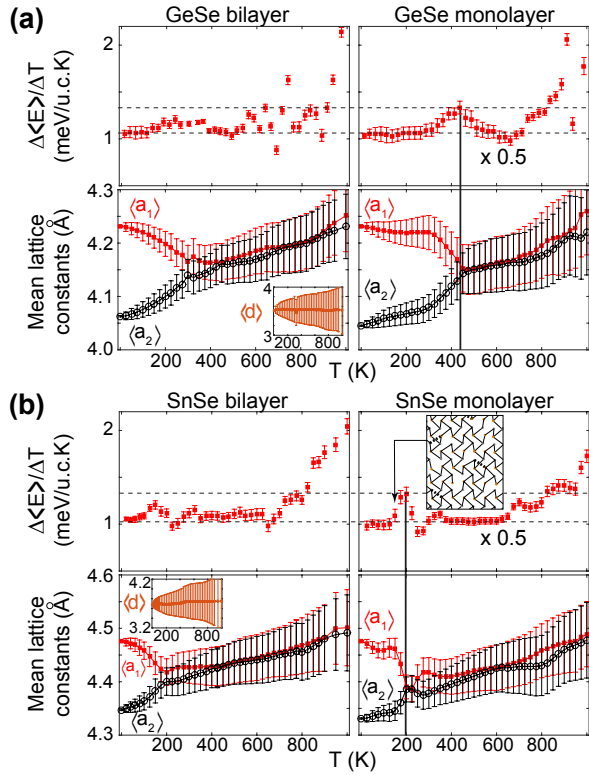


FIG. 1. (Color online.) Finite-difference approximation to  $d\langle E \rangle / dT$  per unit cell (u.c) and  $\langle a_1 \rangle$ ,  $\langle a_2 \rangle$  for (a) GeSe and (b) SnSe BLs and MLs.  $T_c$  is reached when  $\langle a_1 \rangle = \langle a_2 \rangle$ , and it is captured by sharp peaks on monolayer (ML)  $\Delta\langle E \rangle / \Delta T$  subplots highlighted by solid vertical lines.  $\Delta\langle E \rangle / \Delta T$  was scaled by 2 on ML subplots for a direct comparison with BL data (hence the  $\times 0.5$  labels). The average distance among layers  $\langle d \rangle$  for BLs is shown in insets with non-scaled error bars. A structural model showing nearest neighbors is displayed as an inset. (Error bars on  $\langle a_1 \rangle$  and  $\langle a_2 \rangle$  were scaled by 1/6 to make the vertical scale fit within a 0.3 Å vertical range.)

and  $a_2$  towards the right of the  $a_1 = a_2$  line begin to have a finite probability with increasing temperature though, and  $a_1$  and  $a_2$  have a rather homogeneous distribution at  $T_c$ , as seen at the uppermost subplots in Figs. 2(a) and 2(b). A displacive transition would be realized if the yellow spots on the distribution at 25 K in Fig. 2 moved towards the values of  $\langle a_1 \rangle = \langle a_2 \rangle$  with minimal scatter as  $T_c$  is approached from below, so Fig. 2 demonstrates the order-disorder character of the 2D phase transition occurring in these materials conclusively.

We will now show that temperature induces a deformation potential  $U_D$  [23, 24] is induced as a result of the structural evolution. We estimated it from the atomistic fluctuations of the deepest electronic level [25] at finite temperature  $E_l(T)$ ; a state with largest contribution from Se 4s orbitals located at about  $E_l(0) = -17.50$  eV for the GeSe MLs and BLs, and near  $-16.74$  eV for SnSe MLs and BLs at 0 K. The energy location of  $E_l(T)$  decreases with  $T$ , and  $U_D(T)$  in Table I is equal to  $E_l(T) - E_l(0)$  (standard deviations are driven by atomistic fluctuations).

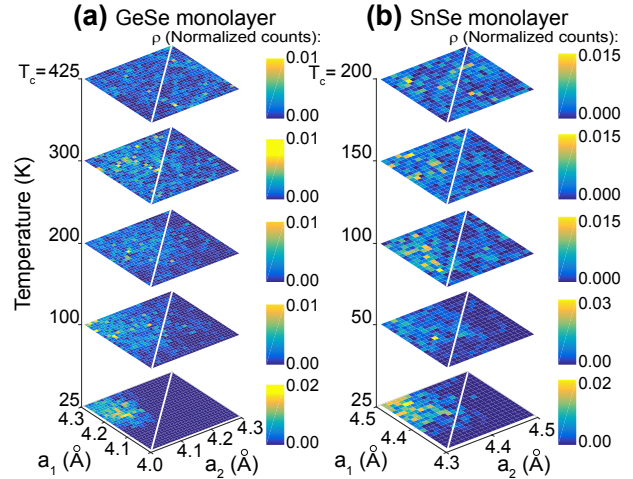


FIG. 2. (Color online.) Probability distribution of lattice constants  $\rho(a_1, a_2)$  for (a) GeSe and (b) SnSe MLs vs.  $T$ :  $\rho$  is sharply defined at low  $T$ . The elastic energy barrier lies along the white diagonal line  $a_1 = a_2$  and the parameter space being explored increases with  $T$  in a random manner, demonstrating the order-disorder nature of the transition.

TABLE I. Deformation potential  $U_D$  vs.  $T$  (meV).

T (K)	25	100	200	300	425
GeSe ML	$-5 \pm 15$	$-47 \pm 21$	$-91 \pm 15$	$-122 \pm 58$	$-138 \pm 55$
GeSe BL	$-8 \pm 15$	$-22 \pm 22$	$-48 \pm 37$	$-115 \pm 31$	$-135 \pm 65$
SnSe ML	$-7 \pm 9$	$-44 \pm 22$	$-85 \pm 36$	$-141 \pm 59$	$-202 \pm 72$
SnSe BL	$+8 \pm 14$	$-35 \pm 34$	$-88 \pm 30$	$-154 \pm 54$	$-205 \pm 72$

Due to the order-disorder nature of the transition, the electronic properties were determined from six individual  $8 \times 8$  supercell structures extracted from the MD runs at 500, 600, 700, 800, 900, and 1000 fs, which provide an even sampling [9]. We focused on structures in thermal equilibrium at 25, 100, 200, 300 and 425 K.

A deformation potential  $U_D$  [23, 24] is induced as a result of the structural evolution. We estimated it from the atomistic fluctuations of the deepest electronic level [25] at finite temperature  $E_l(T)$ ; a state with largest contribution from Se 4s orbitals located at about  $E_l(0) = -17.50$  eV for the GeSe MLs and BLs, and near  $-16.74$  eV for SnSe MLs and BLs at 0 K. The energy location of  $E_l(T)$  decreases with  $T$ , and  $U_D(T)$  in Table I is equal to  $E_l(T) - E_l(0)$  (standard deviations are driven by atomistic fluctuations).

There are no electronic states within the nominal bandgap despite of the two-dimensional disorder discussed so far. This assertion is demonstrated in the leftmost side of columns (i) to (iv) in Fig. 3 from the electronic density of states (DOS) obtained from six  $8 \times 8$  supercells evenly distributed in time at any given temperature, with a  $10 \times 10$  in-plane k-point grid in order to reach a fine energy resolution.

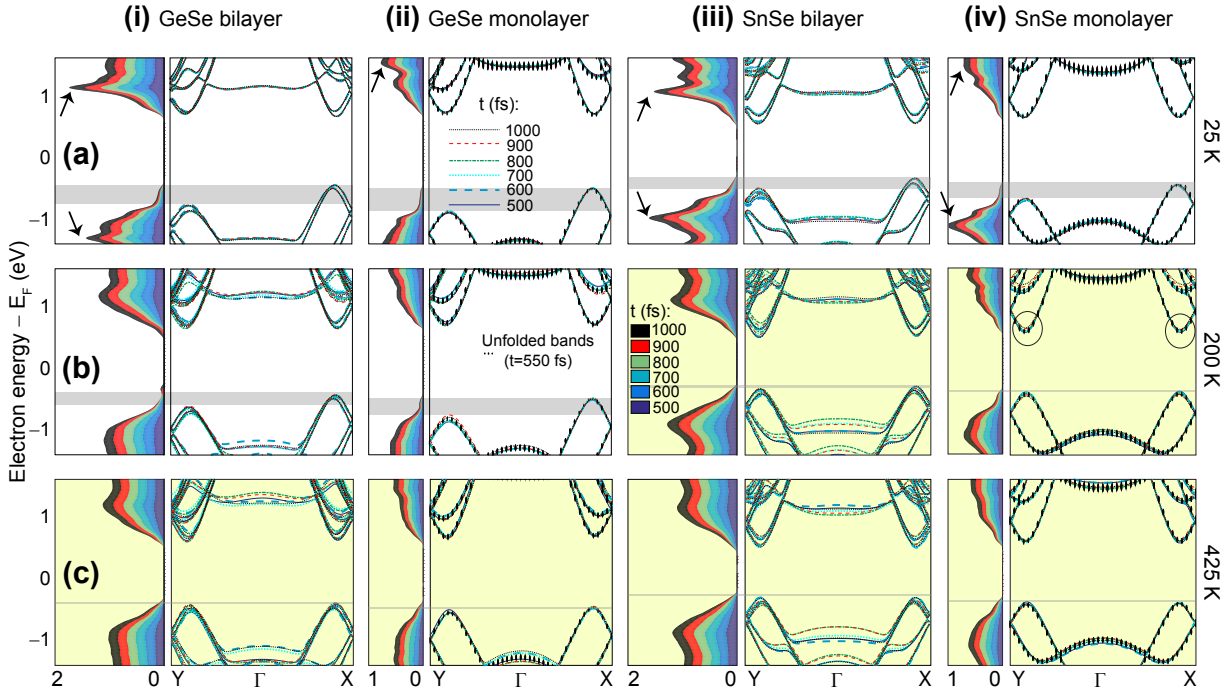


FIG. 3. (Color online.) Electronic DOS and band structures at 500, 600, 700, 800, 900, and 1000 fs for (i) GeSe BL, (ii) GeSe ML, (iii) SnSe BL, and (iv) SnSe ML at (a) 25 K, (b) 200 K, and (c) 425 K. The DOS and band structures become broader with increasing  $T$ , but no in-gap states are seen in the DOS nor the band structures despite of disorder. Subplots with a white (yellow) background were obtained on structures below (at or above) the magnitude of  $T_c$  ( $\langle a_1 \rangle \simeq \langle a_2 \rangle$ ) on ML samples. Band structures show a tendency for the  $X$ - and  $Y$ -points to become equivalent. The zero energy,  $E_F$ , was set at the mid-gap.

The bandgap is reported in Table II, where a reduction of about 75 to 150 meV at  $T_c$  with respect to its magnitude at 0 K is inferred. The DOS shows two additional features: (i) sharp peaks in the DOS at 25 K –indicated by diagonal arrows– that become blurred with increasing temperature, and (ii) a shallow DOS pocket around the valence-band maximum that is emphasized by gray rectangles extending onto band structure subplots.

Band structures in Fig. 3 that complement and provide further support to the information provided by DOS plots were obtained along the  $Y-\Gamma-X$  high-symmetry path in two different ways: (i) from unit cells built from average lattice and basis vectors extracted at a given time-frame from the supercells employed to compute the DOS and without additional optimization of the basis vectors, and (ii) from an unfolding scheme [26, 27] developed for DFT calculations based on numerical atomic orbitals [28, 29]. The sharp peaks on the DOS at 25 K correspond to relatively flat bands located around the  $\Gamma$ -point, whose energy location fluctuates with increasing temperature and makes DOS peaks shallower.

2D materials with reduced structural symmetries originate a novel paradigm in valleytronics in which crystal momentum labels individual valleys one-to-one [30]: in the case of monochalcogenides, the shallow DOS pocket at 25 K ( $\langle a_1 \rangle > \langle a_2 \rangle$ ) corresponds with a hole-valley lo-

TABLE II. Electronic bandgap *vs.*  $T$  (meV).

T (K)	25	100	200	300	425
GeSe ML	$1189 \pm 9$	$1170 \pm 15$	$1130 \pm 17$	$1067 \pm 28$	$1018 \pm 40$
GeSe BL	$1105 \pm 3$	$1091 \pm 20$	$1049 \pm 34$	$974 \pm 58$	$929 \pm 68$
SnSe ML	$1079 \pm 18$	$1043 \pm 36$	$968 \pm 27$	$936 \pm 21$	$893 \pm 28$
SnSe BL	$883 \pm 19$	$861 \pm 24$	$807 \pm 36$	$781 \pm 43$	$725 \pm 42$

cated along the  $\Gamma-X$  line [1, 2, 4] that lies at a higher energy when contrasted to the hole-valley at the  $\Gamma-Y$  line. As shown thus far, MLs and BLs increase their structural symmetry as  $T_c$  is approached from below (Fig. 1), making the  $Y$ - and  $X$ -points equivalent (Fig. 3). This is emphasized by the diminishing height of the (dark) gray rectangles that collapse onto a line at  $T \geq T_c$ .

So far, we have studied electronic properties with the spin-orbit coupling (SOC) turned off. We show in Fig. 4(a) the spin texture at finite temperature once the SOC is included [31]. Explicit calculations show the spin pointing along the  $z$ -direction. In addition, time-reversal symmetry implies a reversal of spin orientations on the other two valleys (located along the  $\Gamma$  to  $-X$  and  $\Gamma$  to  $-Y$  lines). The enhancement of symmetry at  $T_c$  discussed in Fig. 3 continues to be evident at the valleys, and as shown in Fig. 4(b), the spin-polarization becomes drastically de-

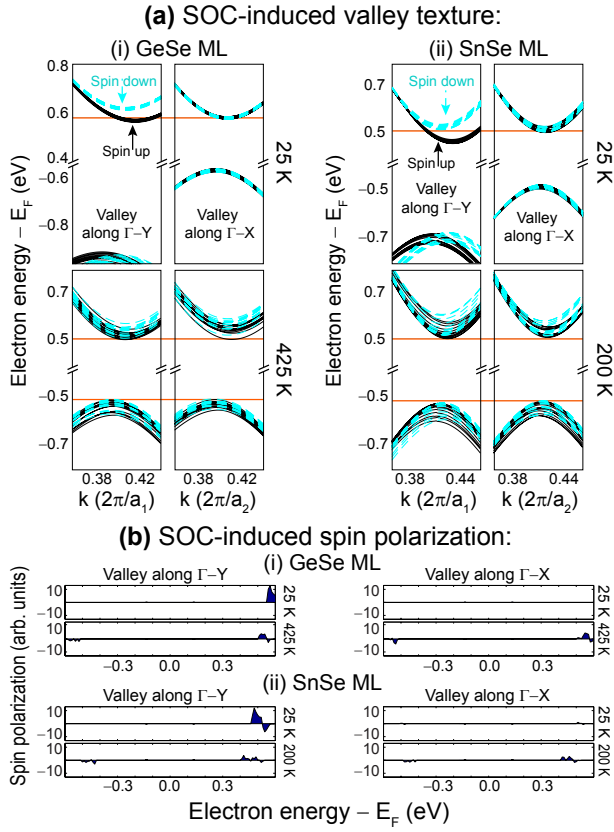


FIG. 4. (Color online.) (a) SOC-induced spin polarization at individual valleys and (b) its degradation with increasing  $T$ .

graded at  $T_c$  due mostly to band broadening. (Bilayers have twice-as-many bands at these energies, making for an even more drastic loss of spin polarization.) We continue to present results with the SOC turned off in the remainder of this Letter.

The mobility  $\mu_{i,d}$  ( $i$  = electron or hole,  $d$  = direction parallel to  $\mathbf{a}_1$  or  $\mathbf{a}_2$ ) resulting from the thermal evolution was estimated as follows [32, 33]:

$$\mu_{i,d} = \frac{2e\hbar^3}{a_1 a_2} \frac{En(T) - En(T=0)}{k_B T m_{i,d}^* m_i^* U_D^2}, \quad (1)$$

where  $a_1$  and  $a_2$  are the lattice constants at 0 K,  $U_D$  the deformation potential,  $En(T)$  the unit cell total energy from the instantaneous unit cell obtained from a structure at temperature  $T$ ,  $m_{i,d}^*$  the (electron or hole) effective mass along the transport direction, and  $m_i^* = \sqrt{m_{i,d}^* m_{i,t}^*}$ , with  $t$  the ‘transverse’ direction. Effective masses were determined from the bands in Fig. 3.

There is a rather small asymmetry in the mobilities along orthogonal directions that lie within error bars. For that reason, we report in Table III its mean magnitude  $\bar{\mu}$  over electron and hole valleys, and over the two orthogonal directions as a function of  $T$ . While  $\bar{\mu}$  becomes smaller with increasing  $T$  in the usual manner [34],

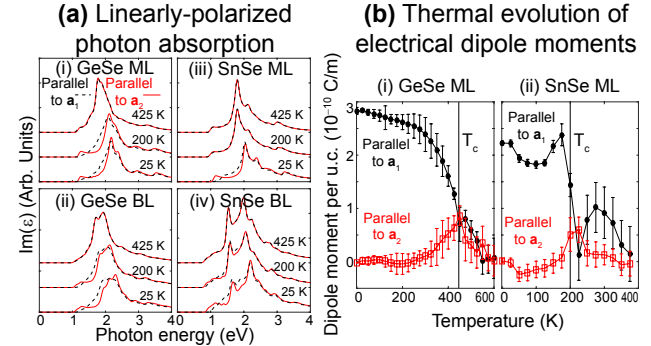


FIG. 5. (Color online.) (a) The (linearly-polarized) optical absorption spectra edge loses its polarization at  $T_c$ . (b) Thermal evolution of the electric dipole moment per unit cell.

TABLE III.  $\bar{\mu}$  vs.  $T$  for GeSe and SnSe MLs ( $\times 10^3 \text{ cm}^2/\text{Vs}$ ).

T (K)	25	100	200	300	425
GeSe	$608 \pm 392$	$8.2 \pm 4.9$	$2.8 \pm 0.8$	$1.5 \pm 0.3$	$1.8 \pm 0.5$
SnSe	$344 \pm 225$	$23.3 \pm 16.8$	$2.4 \pm 1.9$	$0.9 \pm 0.5$	$0.8 \pm 0.3$

the conductance at the valence-band maxima will show a two-fold increase at  $T_c$  as the two hole valleys along the  $\Gamma - Y$  and  $\Gamma - X$  directions align in energy (Fig. 3).

The linearly polarized optical absorption edge discovered in Ref. [1] is key in addressing individual valleys [5]. In Fig. 5(a) we display the average absorption over twelve average unit cells at a given temperature, and establish a vanishing linear polarization of light at the absorption edge  $T_c$ , that is due to the average increase in symmetry (Fig. 1) that makes the hole valleys along orthogonal directions align in energy (Fig. 3).

The binary composition of these materials, and the inversion-asymmetric orientation of individual atoms at the unit cell creates an electric dipole in MLs that is oriented parallel to the longest lattice vector ( $\mathbf{a}_1$ ) [3], resulting in a colossal piezoelectric response at 0 K [6, 35].

But crystalline order is lost at the 2D order-disorder transition [9], making the orientation of these dipoles random at  $T_c$  and the net magnitude of the electric dipole moment equal to zero. This hypothesis is demonstrated in Fig. 5(b) by computing the mean dipole [36] over twelve average unit cells at a given temperature and without any additional optimization of the basis vectors. This was accomplished by feeding the instantaneous structural averages into the VASP code [37] with PBE PAW pseudopotentials [38–40]. In working with instantaneous averaged unit cells, we trade a spatial inhomogeneity by a temporal one. And as  $T_c$  is approached, the relative orientation of the instantaneous average orientation among the atoms in the unit cell fluctuates, and with it the orientation of the dipole moment. The total moment – obtained as an average over 12 individual instantaneous

unit cells– decreases significantly as a result.

To conclude, GeSe and SnSe MLs and BLs undergo a two-dimensional structural transition at finite temperature that alters all material properties.

Y. Y. and L. B. were funded by ONR Grant N00014-12-1-1034. BMF acknowledges support from NSF DMR-1206515. J.F. acknowledges funding from the Spanish MICINN, Grant FIS2012-34858, and European Commission FP7 ITN MOLESCO (Grant No. 606728). Calculations were performed at Arkansas' *Trestles*.

---

\* [sbarraza@uark.edu](mailto:sbarraza@uark.edu)

- [1] G. A. Tritsaris, B. D. Malone, and E. Kaxiras, *J. Appl. Phys.* **113**, 233507 (2013).
- [2] A. K. Singh and R. G. Hennig, *Appl. Phys. Lett.* **105**, 042103 (2014).
- [3] Z. Zhu, J. Guan, D. Liu, and D. Tománek, *ACS Nano* **9**, 8284 (2015).
- [4] L. C. Gomes and A. Carvalho, *Phys. Rev. B* **92**, 085406 (2015).
- [5] A. S. Rodin, L. C. Gomes, A. Carvalho, and A. H. Castro Neto, *Phys. Rev. B* **93**, 045431 (2016).
- [6] R. Fei, W. Li, J. Li, and L. Yang, *Appl. Phys. Lett.* **107**, 173104 (2015).
- [7] A. M. Cook, B. M. Fregoso, F. de Juan, and J. E. Moore, “Design principles for shift current photovoltaics,” ArXiv:1507.08677 [cond-mat.mes-hall].
- [8] T. Morimoto and N. Nagaosa, “Shift current of excitons in noncentrosymmetric crystals,” ArXiv:1512.00549 [cond-mat.mes-hall].
- [9] M. Mehboudi, A. M. Dorio, W. Zhu, A. van der Zande, H. O. H. Churchill, A. A. Pacheco-Sanjuan, E. O. Harriss, P. Kumar, and S. Barraza-Lopez, *Nano Lett.* (2016), article ASAP. DOI:10.1021/acs.nanolett.5b04613.
- [10] X. Mao, A. Souslov, C. I. Mendoza, and T. C. Lubensky, *Nat. Comm.* **6**, 5968 (2014).
- [11] T. C. Lubensky, C. L. Kane, X. Mao, A. Souslov, and K. Sun, *Rep. Prog. Phys.* **78**, 073901 (2015).
- [12] T. Chattopadhyay, J. Pannetier, and H. V. Schnerring, *J. Phys. Chem. Solids* **47**, 879 (1986).
- [13] L.-D. Zhao, S.-H. Lo, Y. Zhang, H. Sun, G. Tan, C. Uher, C. Wolverton, V. P. Dravid, and M. G. Kanatzidis, *Nature* **508**, 373 (2014).
- [14] C. W. Li, J. Hong, A. F. May, D. Bansal, S. Chi, T. Hong, G. Ehlers, and O. Delaire, *Nat. Phys.* **11**, 1063 (2015).
- [15] J. P. Heremans, *Nature Physics* **11**, 990 (2015).
- [16] J. M. Soler, E. Artacho, J. D. Gale, A. Garcia, J. Junquera, P. Ordejon, and D. Sanchez-Portal, *J. Phys.: Condens. Matter* **14**, 2745 (2002).
- [17] R. Car and M. Parrinello, *Phys. Rev. Lett.* **55**, 2471 (1985).
- [18] M. Parrinello and A. Rahman, *Phys. Rev. Lett.* **45**, 1196 (1980).
- [19] J. Junquera, O. Paz, D. Sánchez-Portal, and E. Artacho, *Phys. Rev. B* **64**, 235111 (2001).
- [20] P. Rivero, V. M. Garcia-Suarez, D. Pereniguez, K. Utt, Y. Yang, L. Bellaiche, K. Park, J. Ferrer, and S. Barraza-Lopez, *Comp. Mat. Sci.* **98**, 372 (2015).
- [21] K. Berland and P. Hyldgaard, *Phys. Rev. B* **89**, 035412 (2014).
- [22] One must note, nevertheless, that the value magnitude of  $T_c$  has a slight dependency on the choice of basis set.
- [23] H. Suzuura and T. Ando, *Phys. Rev. B* **65**, 235412 (2002).
- [24] J. V. Sloan, A. A. P. Sanjuan, Z. Wang, C. Horvath, and S. Barraza-Lopez, *Phys. Rev. B* **87**, 155436 (2013).
- [25] S. Barraza-Lopez, M. Kindermann, and M. Y. Chou, *Nano Letters* **12**, 3424 (2012).
- [26] T. B. Boykin and G. Klimeck, *Phys. Rev. B* **71**, 115215 (2005).
- [27] V. Popescu and A. Zunger, *Phys. Rev. Lett.* **104**, 236403 (2010).
- [28] C.-C. Lee, Y. Yamada-Takamura, and T. Ozaki, *Journal of Physics: Condensed Matter* **25**, 345501 (2013).
- [29] J. Ferrer, C. J. Lambert, V. M. Garcia-Suarez, D. Z. Manrique, D. Visontai, L. Oroszlany, R. Rodriguez-Ferradas, I. Grace, S. W. D. Bailey, K. Gillemot, H. Sadeghi, and L. A. Algharagholy, *New J. Phys.* **16**, 093029 (2014).
- [30] P. Rivero, J.-A. Yan, V. M. García-Suárez, J. Ferrer, and S. Barraza-Lopez, *Phys. Rev. B* **90**, 241408 (2014).
- [31] L. Fernandez-Seivane, M. A. Oliveira, S. Sanvito, and J. Ferrer, *Journal of Physics: Condensed Matter* **18**, 7999 (2006).
- [32] S. Takagi, A. Toriumi, M. Iwase, and H. Tango, *IEEE Trans. Electron. Dev.* **41**, 2363 (1994).
- [33] S. Bruzzone and G. Fiori, *Appl. Phys. Lett.* **99**, 222108 (2011).
- [34] R. Fei and L. Yang, *Nano Lett.* **14**, 2884 (2014).
- [35] L. C. Gomes, A. Carvalho, and A. H. Castro Neto, *Phys. Rev. B* **92**, 214103 (2015).
- [36] R. D. King-Smith and D. Vanderbilt, *Phys. Rev. B* **47**, 1651 (1993).
- [37] G. Kresse and J. Furthmüller, *Phys. Rev. B* **54**, 11169 (1996).
- [38] J. Perdew, K. Burke, and M. Ernzerhof, *Phys. Rev. Lett.* **77**, 3865 (1996).
- [39] P. E. Blochl, *Phys. Rev. B* **50**, 17953 (1994).
- [40] G. Kresse and D. Joubert, *Phys. Rev. B* **59**, 1758 (1999).